P H Y S I C A L   R E V I E W   L E T T E R S

Strongly Enhanced Pinning of Magnetic Vortices in Type-II Superconductors by Conformal Crystal Arrays

D. Ray,[1,2] C. J. Olson Reichhardt,[2] B. Jankó,[1] and C. Reichhardt[2]

[1]*Department of Physics, University of Notre Dame, Notre Dame, Indiana 46556, USA*
[2]*Theoretical Division, Los Alamos National Laboratory, Los Alamos, New Mexico 87545, USA*
(Received 3 October 2012; published 24 June 2013)

Conformal crystals are nonuniform structures created by a conformal transformation of regular two-dimensional lattices. We show that gradient-driven vortices interacting with a conformal pinning array exhibit substantially stronger pinning effects over a much larger range of field than found for random or periodic pinning arrangements. The pinning enhancement is partially due to matching of the critical flux gradient with the pinning gradient, but the preservation of local ordering in the conformally transformed hexagonal lattice and the arching arrangement of the pinning also play crucial roles. Our results can be generalized to a wide class of gradient-driven interacting particle systems such as colloids on optical trap arrays.

One of the most important problems for applications of type-II superconductors is how to create high critical currents or strong vortex pinning over a wide range of applied magnetic fields [1]. For over sixty years, it has been understood that the ground state vortex structure is a hexagonal lattice [2], so many methods have been developed to increase the critical current using uniform pinning arrays that incorporate periodicity to match the vortex structure [3–13]. The pinning is enhanced at commensurate fields when the number of vortices equals an integer multiple of the number of pinning sites, but away from these specific matching fields, the enhancement of the critical current is lost [14]. Efforts to enhance the pinning at incommensurate fields have included the use of quasicrystalline substrates [15] or diluted periodic arrays [16–20], where studies show that new types of noninteger commensurate states can arise in addition to the integer matching configurations. Hyperbolic tessellation arrays were also recently considered [21].

Part of the problem is the fact that under an applied current, the vortex structure does not remain uniform but instead develops a Bean-like flux gradient [22]: the vortex density is highest at the edges of the sample when the magnetic field is increased, and highest in the center of the sample when the magnetic field is removed and only trapped flux remains inside the sample. As a consequence, a portion of the pinning sites in uniform pinning arrays is not fully occupied, suggesting that a more optimal pinning arrangement should include some type of density gradient to match the critical flux gradient. Here, we show that a novel type of pinning array, based on a structure known as a conformal crystal, produces a much higher critical current over a much wider range of magnetic fields than any pinning geometry considered up until now. Conformal crystals not only have a density gradient but also preserve

the local ordering normally associated with periodic pinning arrays.

Conformal crystals are a class of two-dimensional (2D) structures created by the application of a conformal (angle-preserving) transformation to a regular lattice in the complex plane [23,24]. Figure 1 illustrates a conformal crystal
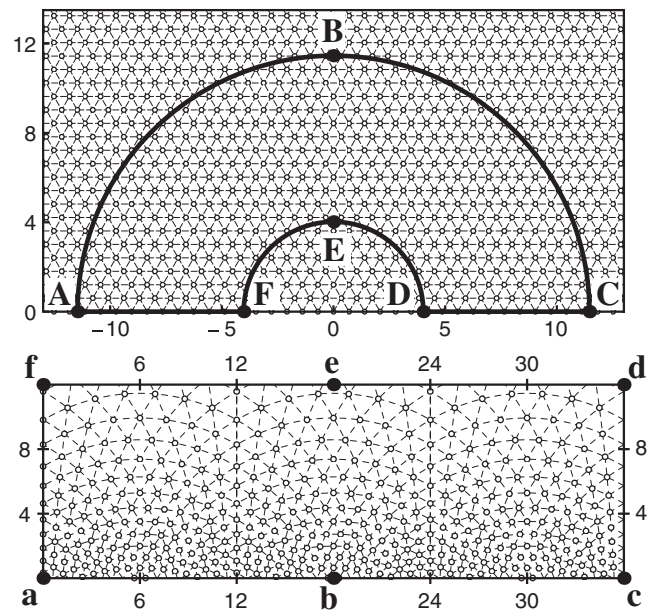

FIG. 1. A conformal transformation is applied to the semi-annular section of a regular hexagonal lattice shown in (a) to create the conformal crystal structure shown in (b) (see the Supplemental Material [25]). Points A–F in (a) are mapped by the transformation to points a–f in (b), respectively. The straight contour lines connecting nearest neighbor lattice points in (a) are bent into arcs in (b), but the local sixfold ordering of the lattice points is maintained. Pinning sites are placed at the vertices formed by the intersections of the contour lines in (b).

obtained via the transformation of a hexagonal lattice [25]. The contour lines connecting nearest neighbors, which are straight lines for the original hexagonal lattice, are bent into arcs but still cross at angles of $\pi/3$, preserving the sixfold coordination of individual pinning sites in spite of the clear density gradient. To create a pinning lattice, we place pinning sites at the vertex locations where the contour lines intersect. Conformal crystal structures have been studied experimentally for repulsively interacting magnetic spheres confined to a 2D container that is tilted so that the gravitational force on the particles produces a mechanically stable but nonuniform crystal [24]. Other systems where conformal crystals arise include foams under an external field [26,27] and large arrays of classical Coulomb charges in confined circular potentials where local triangular ordering occurs along curved lattice lines [28].

Simulation.—We conduct a flux gradient density simulation of the type previously used to study vortex critical states and magnetization with random [29,30] and periodic pinning arrays [14], featuring a 2D slice (in the x-y plane) of a $T = 0$ superconducting slab, with rigid vortices parallel to the sample edge ($\mathbf{H} = H\hat{z}$). We work in the London limit of vortices with pointlike cores. Figure 2 shows our simulation geometry, featuring an outer pin-free "external" region surrounding a central pinned "sample" region that consists of two conformal crystals placed with their highest density regions adjacent to the pin-free region. Details on the construction of the conformal crystal are given in the Supplemental Material [25]. We use periodic boundary conditions in the x and y directions and consider a $36\lambda \times 36\lambda$ system with a pinned region extending from $x = 6\lambda$ to 30λ, where λ is the penetration depth. This geometry was previously shown to be large enough to capture accurately the behavior of the magnetization curves [14,29,30].

The dynamics of vortex i are obtained by integrating the overdamped equation $\eta(d\mathbf{R}_i/dt) = \mathbf{F}_i^{vv} + \mathbf{F}_i^{vp} + \mathbf{F}^d$.
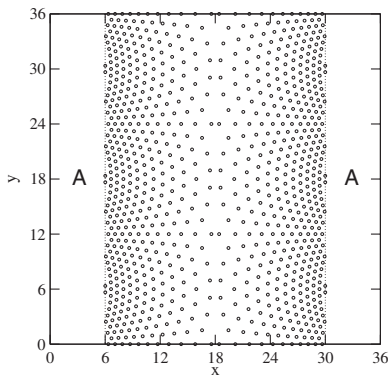

FIG. 2. The gradient-driven sample geometry consists of two conformal crystals facing each other in the pinned region. Open circles are pinning site locations. Vortex addition and subtraction occurs in the pin-free region labeled A.

Here, η is the damping constant which is set equal to unity. The vortex-vortex interaction force is $\mathbf{F}_i^{vv} = \sum_{j=1}^{N_v} s_i s_j F_0 K_1(R_{ij}/\lambda)\hat{\mathbf{R}}_{ij}$, where K_1 is the modified Bessel function, $\mathbf{R}_i$ is the location of vortex i, $R_{ij} = |\mathbf{R}_i - \mathbf{R}_j|$, $\hat{\mathbf{R}}_{ij} = (\mathbf{R}_i - \mathbf{R}_j)/R_{ij}$, $F_0 = \phi_0^2/(2\pi\mu_0\lambda^3)$, and ϕ_0 is the flux quantum. The sign prefactor s_i is $+1$ for a vortex and -1 for an antivortex. The pinning sites are modeled as N_p nonoverlapping parabolic traps with $\mathbf{F}_i^{vp} = \sum_{k=1}^{N_p}(F_p r_{ik}^p/r_p)\Theta((r_p - r_{ik}^p)/\lambda)\hat{\mathbf{R}}_{ik}^p$, where $\mathbf{R}_k^p$ is the location of pinning site k, $r_{ik}^p = |\mathbf{R}_i - \mathbf{R}_k^p|$, $\hat{\mathbf{R}}_{ik}^p = (\mathbf{R}_i - \mathbf{R}_k^p)/r_{ik}^p$, Θ is the Heaviside step function, r_p is the pinning radius, and F_p is the pinning strength. Unless otherwise noted, we take $r_p = 0.12\lambda$ and $F_p = 0.55F_0$, placing us well outside the collective pinning regime. In this work, we always maintain the pinning density at a nominal value of $1.0\lambda^{-2}$, corresponding to $N_p = 864$ pins. $\mathbf{F}^d = F_d\hat{x}$ represents an external driving force arising from an applied current, which is used to measure transport properties; this is kept at zero for all magnetization measurements. All forces are measured in units of F_0 and all lengths in units of λ. The flux density H in the unpinned region is measured in units of H_ϕ, the field at which the average unit density of vortices equals the average unit density of pinning sites.

To perform a complete field sweep, we begin with zero vortex density and then quasistatically add vortices in the unpinned region (labeled A in Fig. 2) at randomly chosen nonoverlapping positions. As the vortex density increases in the pin-free region, the vortices drive themselves into the pinned region due to their own repulsive interactions, creating a flux density gradient [14,29,30]. We then reverse the field by first removing vortices from the pin-free region and then adding antivortices, which repel each other but are attracted to vortices. When a vortex and antivortex come within 0.3λ of each other, they are both removed from the system to simulate an annihilation event. To complete an entire magnetization loop, we continue to add antivortices until the external field reaches its most negative value, and then remove antivortices from the pin-free region to bring the external field back up to zero. The average magnetization M is the difference between the flux density H in the unpinned region and B in the pinned region $M = -(1/4\pi V)\int(H - B)dV$, where V is the sample area. The critical current J_c can be derived from the magnetization curve using the Bean critical state model [22], as described in Refs. [31–33].

Results.—In Fig. 3, we plot an example of complete hysteresis loops M versus H/H_ϕ for the conformal pinning array (CPA) and arrays with randomly distributed pins. Each sample contains the same number N_p of pinning sites of equal size and strength. In comparison with random pinning (inner curve), we find that M is much higher at all fields for the CPA (outer curve). In Figs. 4(a) and 4(b), we plot the magnetization loop half-width M_{HW}
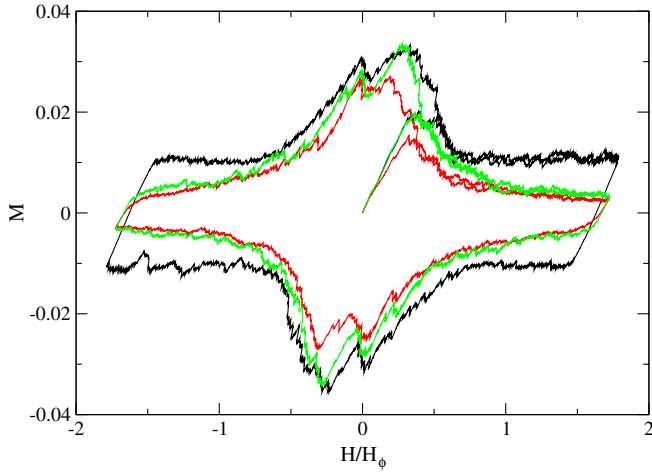
FIG. 3 (color online).   The magnetization M versus H/H_ϕ. The outer dark (black) curve represents a sample with a CPA, the inner light (red) curve a sample with a uniformly dense random arrangement of pinning sites, and the middle light (green) curve a random arrangement of pinning sites with a pinning gradient equivalent to the CPA.

FIG. 4 (color online).   (a),(b) M_{HW}, the half-width of the magnetization loop, measured at $H/H_\phi = 1.0$ (filled symbols) and at $H/H_\phi = 1.4$ (open symbols) and normalized to M_{HW} for the random pinning array (squares). The circles represent the CPA, the triangles the random array with CPA-equivalent pinning gradient. (a) M_{HW} versus F_p for fixed $r_p = 0.12$. (b) M_{HW} versus r_p for fixed $F_p = 0.55$. (c) $\langle V_x \rangle$ versus F_d for vortices driven across a CPA (right curve, black), a random array (center curve, red), and a random array with a pinning gradient (left curve, green). (d) Magnetization loops for the CPA (outer curve, black) compared to periodic pinning arrays, square (center curve, blue) and triangular (inner curve, purple), at $F_p = 0.55$ and $r_p = 0.12$.

measured at an intermediate field $H/H_\phi = 1.0$ and a high field $H/H_\phi = 1.4$, for a variety of pinning sizes and strengths. The CPA consistently enhances the magnetization by a factor of 4 relative to random pinning. The flux profiles plotted in the Supplemental Material Fig. 1 [25] show that the random array produces a Bean-like profile that becomes shallower as H increases. In contrast, at higher fields, the CPA does not have a uniform flux gradient but instead develops a double slope profile, with a larger flux gradient near the edge of the sample and a much shallower or nearly flat flux profile in the center of the sample. As H increases, the sharper slope region decreases in width and is replaced by the shallow slope region. Consequently, the CPA maintains a large M even for high values of H.

Since the CPA has a pinning gradient, it could be possible that any type of pinning array with an equivalent gradient would also exhibit a pinning enhancement compared to uniform pinning arrays and could be just as efficient at pinning as the CPA. We find that this is not the case. In Figs. 3, 4(a), and 4(b), we show magnetization results for a random pinning array with pinning gradient equivalent to the CPA. The random pinning with gradient exhibits a modest enhancement of M compared to the uniform random pinning array but trails the CPA significantly for all but the very lowest fields: as Figs. 4(a) and 4(b) indicate, the loop half-width for the CPA remains larger by a factor of 3 to 4. This result indicates that other properties of the CPA, and not merely the pinning gradient, are largely responsible for the enhanced pinning. We find that the structure of the CPA suppresses certain modes of vortex motion. For example, in random pinning arrays, the distribution of pins is inhomogeneous; as a consequence,
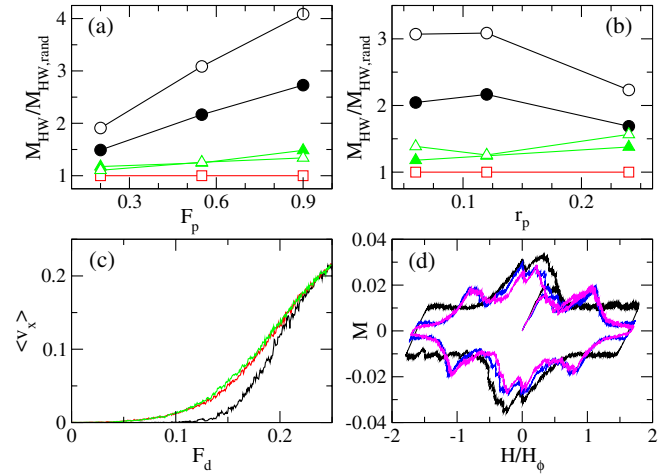
persistent riverlike vortex flow patterns arise through regions where the pinning density is slightly lower than average [30]. In contrast, because the CPA is an ordered structure, it lacks any such weak spots through which vortices would prefer to flow.

To confirm the effectiveness of the CPA at enhancing the critical current compared to random pinning arrays, we examine transport properties by field cooling the system at $H/H_\phi = 1$, driving the vortices with a slowly increasing force $\mathbf{F}_d = F_d\hat{\mathbf{x}}$, and measuring the average vortex velocity in the drive direction $\langle V_x \rangle$ to produce the equivalent of an experimental $V(I)$ curve [34]. The transport geometry and simulation method are detailed in the Supplemental Material [25]. Figure 4(c) shows velocity-force curves for the CPA and random pinning arrays. The CPA clearly exhibits an increased resistance to flux flow, with a much larger depinning threshold. Above depinning, vortices continue to move more slowly through the CPA for a wide range of driving force.

We next address whether the conformal pinning arrays produce higher pinning compared to other nonrandom pinning arrays. In Fig. 4(d), we plot M versus H/H_ϕ for the CPA and for square and triangular periodic pinning arrays with the same average pinning density and strength. The CPA has the highest value of M over most of the range of H/H_ϕ except at the first matching field, where M is enhanced in the periodic pinning arrays due to a
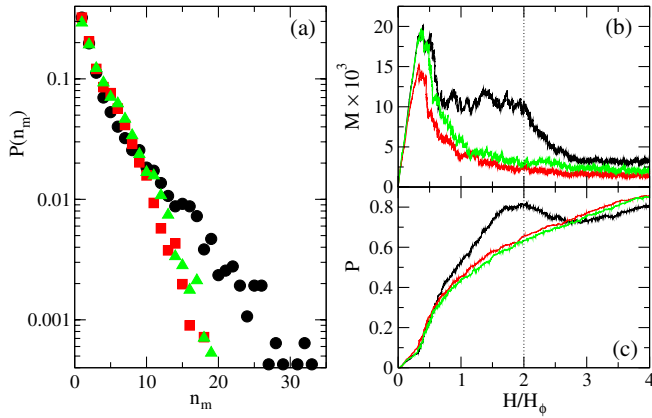
FIG. 5 (color online).   (a) $P(n_m)$, the distribution of the number of vortices n_m in individual avalanches occurring as the field H/H_ϕ is raised from 0.65 to 2.0, for the CPA (circles), uniform random pinning (squares), and random pinning with gradient (triangles). (b),(c) High-field behavior of pinning arrays on the initial ramp-up only: in (b), magnetization M, and in (c), the fraction of occupied pinning sites P. The CPA is represented by the upper (black) curve, the uniform random array by the lower (red) curve, and random with gradient by the middle (green) curve. The dotted line indicates $H/H_\phi = 2$, where M and P both drop for the CPA.

commensurability effect [14]. There are no peaks or other anomalies in M for the CPA since the triangular ordering in this array is only local. This shows that although a periodic pin structure can strongly enhance the pinning, the enhancement occurs only for a very specific matching field. In contrast, the CPA produces a significant enhancement of the pinning over a very broad range of fields, extending well above the first matching field. This enhancement arises not only from the presence of a pinning gradient, which periodic pinning lacks, but also because the arching structure of the CPA blocks easy-flow channels, which are present along the symmetry directions of periodic pinning arrays [35,36] and cause a drop in the critical current above a commensurate field.

To gain further insight into the effectiveness of the CPA, we consider the details of vortex entry. Since the vortex system is maintained in a critical state when measuring M, the vortex motion can be characterized by avalanche dynamics [37]. In Fig. 5(a), we show the probability distribution $P(n_m)$ for the number n_m of vortices participating in individual avalanche events during ramp-up. For the CPA, $P(n_m)$ is more heavily weighted toward large events compared to the random arrays. This is due to the suppression of easy vortex entry channels by the CPA. In order for vortices to enter the CPA sample, considerable pressure must build up in the external region, and the resulting avalanches are larger.

Finally, we characterize the conditions under which the effectiveness of the CPA begins to decrease. In Fig. 5(b), we compare M versus H/H_ϕ for the CPA and uniform random arrays up to $H/H_\phi = 4.0$. The enhanced pinning for the CPA is most pronounced below $H/H_\phi = 2.0$; above this field, M remains larger for the CPA than for the random pinning array, but the size of the enhancement is reduced. In Fig. 5(c), we plot the corresponding pin occupancy P, which is the fraction of pinning sites occupied by vortices. For the random pinning array, P monotonically increases over the entire range of H/H_ϕ. In contrast, after running well above the P value for the random pinning array at lower fields, P for the CPA rolls over and begins to decrease with increasing field above $H/H_\phi \approx 2$. This is the same field at which the higher gradient region seen in the Supplemental Material Fig. 1(a) begins to disappear from the sample, as shown in the Supplemental Material Fig. 2 [25]. Since the pinning density at the edge of our CPA is approximately 2, all of the pinning sites near the edge of the sample become occupied for $H/H_\phi \approx 2$. For $H/H_\phi < 2$, the vortex density just outside the sample can be matched purely by pinned vortices just inside, but for $H/H_\phi > 2$, pressure from outside the sample forces interstitial vortices to enter, depinning some of the vortices already present and producing a drop in P and M.

The random pinning array always has empty pinning sites near the edge of the sample in places where two pins happen to be so close together that the vortex-vortex interaction energy would be prohibitively high if both pins were occupied simultaneously. As the field increases, these pinning sites gradually become occupied. Even though P for the CPA falls below P for the random array at higher fields, the pinning enhancement remains significantly stronger for the CPA, as the presence of weak spots in the random array facilitates vortex entry deep into the sample region.

Conclusion.—We demonstrate strongly enhanced vortex pinning by a conformal crystal array of pinning sites. The conformal crystal is constructed by a conformal transformation of a hexagonal lattice, producing a nonuniform structure with a gradient where the local sixfold coordination of the pinning sites is preserved, and with an arching effect. The conformal pinning arrays produce significantly enhanced pinning over a much wider range of field than that found for other pinning geometries with an equivalent number of pinning sites, such as random, square, and triangular. We show that the pinning enhancement is not simply due to the pin density gradient but is also due to the preservation of the local ordering of the pinning sites and to the arching pin arrangement, which prevent the formation of easy channels of vortex flow. The pinning enhancement we find is substantial and will be important for a wide range of superconductor applications and flux control. The effects of conformal crystalline substrates on ordering or dynamics of a monolayer of particles could also be studied for vortices in Bose-Einstein condensates on optical lattices [38] or colloidal particles on optically created substrate arrays [39]. The enhanced pinning also suggests that

conformal arrays could be used to increase friction for particle-surface interactions.

———————

[1] G. Blatter, M. V. Feigel'man, V. B. Geshkenbein, A. I. Larkin, and V. M. Vinokur, Rev. Mod. Phys. **66**, 1125 (1994).

[2] A. A. Abrikosov, Rev. Mod. Phys. **76**, 975 (2004).

[3] M. Baert, V. V. Metlushko, R. Jonckheere, V. V. Moshchalkov, and Y. Bruynseraede, Phys. Rev. Lett. **74**, 3269 (1995).

[4] V. Metlushko, U. Welp, G. W. Crabtree, R. Osgood, S. D. Bader, L. E. DeLong, Z. Zhang, S. R. J. Brueck, B. Ilic, K. Chung, and P. J. Hesketh, Phys. Rev. B **60**, R12585 (1999).

[5] S. B. Field, S. S. James, J. Barentine, V. Metlushko, G. Crabtree, H. Shtrikman, B. Ilic, and S. R. J. Brueck, Phys. Rev. Lett. **88**, 067003 (2002); A. N. Grigorenko, S. J. Bending, M. J. Van Bael, M. Lange, V. V. Moshchalkov, H. Fangohr, and P. A. J. de Groot, ibid. **90**, 237001 (2003).

[6] U. Welp, X. L. Xiao, J. S. Jiang, V. K. Vlasko-Vlasov, S. D. Bader, G. W. Crabtree, J. Liang, H. Chik, and J. M. Xu, Phys. Rev. B **66**, 212507 (2002); U. Welp, X. L. Xiao, V. Novosad, and V. K. Vlasko-Vlasov, Phys. Rev. B **71**, 014505 (2005).

[7] G. Karapetrov, J. Fedor, M. Iavarone, D. Rosenmann, and W. K. Kwok, Phys. Rev. Lett. **95**, 167002 (2005).

[8] J. I. Martín, M. Vélez, A. Hoffmann, I. K. Schuller, and J. L. Vicent, Phys. Rev. Lett. **83**, 1022 (1999); W. J. Zhang et al., Europhys. Lett. **99**, 37 006 (2012).

[9] J. I. Martín, M. Vélez, J. Nogués, and I. K. Schuller, Phys. Rev. Lett. **79**, 1929 (1997); D. J. Morgan and J. B. Ketterson, ibid. **80**, 3614 (1998); J. E. Villegas, E. M. Gonzalez, Z. Sefrioui, J. Santamaria, and J. L. Vicent, Phys. Rev. B **72**, 174512 (2005).

[10] K. Harada, O. Kamimura, H. Kasai, T. Matsuda, A. Tonomura, and V. V. Moshchalkov, Science **274**, 1167 (1996); C. Reichhardt, C. J. Olson, and F. Nori, Phys. Rev. B **57**, 7937 (1998); G. R. Berdiyorov, M. V. Milosevic, and F. M. Peeters, Phys. Rev. Lett. **96**, 207001 (2006).

[11] S. Goldberg, Y. Segev, Y. Myasoedov, I. Gutman, N. Avraham, M. Rappaport, E. Zeldov, T. Tamegai, C. Hicks, and K. Moler, Phys. Rev. B **79**, 064523 (2009); G. Shaw, B. Bag, S. S. Banerjee, H. Suderow, and T. Tamegai, Supercond. Sci. Technol. **25**, 095016 (2012).

[12] J. I. Vestgarden, V. V. Yurchenko, R. Wördenweber, and T. H. Johansen, Phys. Rev. B **85**, 014516 (2012).

[13] I. Swiecicki, C. Ulysse, T. Wolf, R. Bernard, N. Bergeal, J. Briatico, G. Faini, J. Lesueur, and J. E. Villegas, Phys. Rev. B **85**, 224502 (2012).

[14] C. Reichhardt, J. Groth, C. J. Olson, S. B. Field, and F. Nori, Phys. Rev. B **54**, 16 108 (1996).

[15] V. Misko, S. Savel'ev, and F. Nori, Phys. Rev. Lett. **95**, 177007 (2005); M. Kemmler, C. Gürlich, A. Sterck, H.

Pöhler, M. Neuhaus, M. Siegel, R. Kleiner, and D. Koelle, Phys. Rev. Lett. **97**, 147003 (2006); A. V. Silhanek, W. Gillijns, V. V. Moshchalkov, B. Y. Zhu, J. Moonens, and L. H. A. Leunissen, Appl. Phys. Lett. **89**, 152507 (2006); J. E. Villegas, M. I. Montero, C.-P. Li, and I. K. Schuller, Phys. Rev. Lett. **97**, 027002 (2006); C. Reichhardt and C. J. Olson Reichhardt, Phys. Rev. Lett. **106**, 060603 (2011).

[16] C. Reichhardt and C. J. Olson Reichhardt, Phys. Rev. B **76**, 094512 (2007).

[17] M. Kemmler, D. Bothner, K. Ilin, M. Siegel, R. Kleiner, and D. Koelle, Phys. Rev. B **79**, 184509 (2009).

[18] Y. J. Rosen, A. Sharoni, and I. K. Schuller, Phys. Rev. B **82**, 014509 (2010).

[19] C. Reichhardt and C. J. Olson Reichhardt, Phys. Rev. B **76**, 064523 (2007).

[20] A. D. Thakur, S. Ooi, S. P. Chockalingam, J. Jesudasan, P. Raychaudhuri, and K. Hirata, Appl. Phys. Lett. **94**, 262501 (2009).

[21] V. R. Misko and F. Nori, Phys. Rev. B **85**, 184506 (2012).

[22] C. P. Bean, Phys. Rev. Lett. **8**, 250 (1962); Rev. Mod. Phys. **36**, 31 (1964).

[23] P. Pieranski, in Phase Transitions in Soft Condensed Matter, edited by T. Riste and D. Sherrington (Plenum, New York, 1989), p. 45; F. Rothen, P. Pieranski, N. Rivier, and A. Joyet, Eur. J. Phys. **14**, 227 (1993).

[24] F. Rothen and P. Pieranski, Phys. Rev. E **53**, 2828 (1996).

[25] See Supplemental Material at http://link.aps.org/supplemental/10.1103/PhysRevLett.110.267001 for details of the construction of the conformal array, transport measurements, and flux profiles.

[26] W. Drenckhan, D. Weaire, and S. J. Cox, Eur. J. Phys. **25**, 429 (2004).

[27] M. Mancini and C. Oguey, Eur. Phys. J. E **17**, 119 (2005).

[28] A. Mughal and M. A. Moore, Phys. Rev. E **76**, 011606 (2007).

[29] C. Reichhardt, C. J. Olson, J. Groth, S. Field, and F. Nori, Phys. Rev. B **52**, 10441 (1995).

[30] C. Reichhardt, C. J. Olson, J. Groth, S. B. Field, and F. Nori, Phys. Rev. B **53**, R8898 (1996).

[31] A. M. Campbell and J. E. Evetts, Adv. Phys. **21**, 199 (1972).

[32] S. Senoussi, J. Phys. III (France) **2**, 1041 (1992).

[33] M. Daeumling, J. M. Seuntjens, and D. C. Larbalestier, Nature (London) **346**, 332 (1990).

[34] C. J. Olson, C. Reichhardt, and F. Nori, Phys. Rev. Lett. **81**, 3757 (1998).

[35] A. V. Silhanek, J. Gutierrez, R. B. G. Kramer, G. W. Ataklti, J. Van de Vondel, V. V. Moshchalkov, and A. Sanchez, Phys. Rev. B **83**, 024509 (2011).

[36] C. Reichhardt and C. J. Olson Reichhardt, Phys. Rev. B **79**, 134501 (2009).

[37] C. J. Olson, C. Reichhardt, and F. Nori, Phys. Rev. B **56**, 6175 (1997).

[38] S. Tung, V. Schweikhard, and E. A. Cornell, Phys. Rev. Lett. **97**, 240402 (2006).

[39] P. T. Korda, G. C. Spalding, and D. G. Grier, Phys. Rev. B **66**, 024504 (2002); K. Mangold, P. Leiderer, and C. Bechinger, Phys. Rev. Lett. **90**, 158302 (2003).